The State Research Center of Russian Federation
BUDKER INSTITUTE OF NUCLEAR PHYSICS

V. Kiselev, E. Levichev,
V. Sajaev, V. Smaluk

NONLINEAR BEAM DYNAMICS STUDY AT VEPP-4M

Budker INP 96-67

NOVOSIBIRSK
1996

Nonlinear beam dynamics study at VEPP-4M

V. Kiselev, E. Levichev,
V. Sajaev, V. Smaluk

Budker Institute of Nuclear Physics SB RAS
630090 Novosibirsk, Russia

Abstract

Nonlinear dynamics of transverse beam motion has been studied experimentally at the VEPP-4M electron-positron collider. Two aspects of nonlinear beam behaviour described in this paper are the amplitude dependent tune shift and the phase space trajectories near nonlinear resonances. The measurement results are presented and compared with the theoretical prediction.

1 Introduction

Nonlinear dynamics experiments were performed at VEPP-4M storage ring in 1995-1996. The main goals of these experiments were to study the essential aspects of the single particle dynamics (phase space distortion, amplitude dependent tune shift and the dynamic aperture limitation); to find the way to control the nonlinear effects, and to check the validity of theoretical prediction.

This paper concerns the first two topics: the phase space topology and nonlinear detuning study. The motion of the beam center of mass was measured turn-by-turn after excitation of the coherent betatron oscillations by fast kicker magnet. Two ways of the phase trajectories plotting were examined: by two BPM stations with the $\pi/2$ betatron phase advance between them and by single BPM. FFT applied to the coordinate array provides a significant noise reduction and an increase of the phase space distortion resolution. Amplitude-dependent tune shift was studied for both sextupole and octupole perturbation. The experimental data agree quite well with the tracking simulation and simple model prediction.

2 Hardware description

VEPP-4M storage ring is a 6 GeV racetrack electron-positron collider with a circumference of 366 m. The study was performed at the injection energy of 1.8 GeV. The relevant parameters of VEPP-4M at this energy are given in the Table:

Energy	1.8 GeV
Revolution period	1.2 μs
Betatron tunes (h/v)	8.620/7.560
Natural chromaticity (h/v)	-13.6/-20.7
Horizontal emittance	35 nm-rad
Rms beam bunch length	6 cm
Damping times (h/v/long.)	35 ms/70 ms/70 ms

To produce the coherent transverse motion, the beam is kicked vertically or horizontally by pulsed electromagnetic kickers. The pulse duration is 50 ns for the horizontal kicker and

150 ns for the vertical one. The oscillation of the beam centroid and beam intensity are measured turn-by-turn with a beam position monitor (BPM) for up to 8192 revolutions. The rms displacement resolution is $\sigma_{x,z} \simeq 70\mu$m in 1 to 5 mA beam current range.

The following sources of the magnetic field nonlinearity were taken into account for the theoretical prediction:

1. 32 vertical and horizontal sextupole corrections distributed along the magnets in the arcs (two families, DS and FS).
2. Short sextupoles $SES2$, $NES2$ and $SES3$, $NES3$ located symmetrically around the interaction point.
3. Quadratic field component produced by the arc magnets pole shape (two families, SSF and SSD).
4. Octupole correction coils incorporated in the arc magnets main coils (32 corrections, two families, SRO and NRO).

The main parameters of the nonlinear elements mentioned above are listed in the Table:

Name	No	Length (cm)	d^2B/dx^2 (G/cm^2)
SSD	32	111.39	-1.68
SSF	32	111.31	1.11
$SES2/NES2$	4	20	9.25
$SES3/NES3$	2	20	-16.25
FS	32	34.2	5.24
DS	32	34.2	-9.25

Because of the high beta-function values ($\simeq$120 m), the bulk of natural chromaticity of the ring is produced by the final focus quadrupoles ($\simeq$50% in horizontal plane and $\simeq$60 % in vertical plane). Hence, we can expect that the influence of the SES/NES sextupoles on the nonlinear dynamics is emphasized.

3 Phase space trajectories

There are two BPMs with the horizontal betatron phase advance $\simeq \pi/2$ between them available in the turn-by-turn mode at VEPP-4M. To study the phase space topology, we were tracked the motion of the beam centroid in two ways: a) by using two BPMs and b) by a single BPM station [2].

Let us consider the horizontal betatron oscillation at the BPM azimuth

$$x(n) = a\beta_x^{1/2} \cos 2\pi n\nu_x,$$
$$x'(n) = -a/\beta_x^{1/2}[\alpha_x \cos 2\pi n\nu_x + \sin 2\pi n\nu_x], \quad (1)$$

where $\alpha_x = -1/2\beta_x'(s)$ and $\beta_x(s)$ are the betatron functions and phase advance for nth turn equals $2\pi n\nu_x$. This expression can be rewritten in the form

$$x'(n) = [x_{\pi/2}(n) - \alpha_x x(n)]/\beta_x,$$

where $x_{\pi/2}(n)$ is the coordinate that would be measured by the BPM placed at the azimuth which corresponds to the following conditions: (i) α_x, β_x here are the same as for the first BPM, (ii) the betatron phase shift between two BPMs is exactly $\pi/2$. Introducing the "angle-action" variables (J_x, ϕ_x) [1] and substituting (1) we can obtain

$$J_x(n) = (x^2_{\pi/2}(n) + x^2(n))/2\beta_x, \qquad (2)$$
$$\tan\phi_x(n) = x_{\pi/2}(n)/x(n).$$

One can see that α_x is canceled from the expression for $J_x(\phi_x)$ and phase curves demonstrate a "mere" nonlinear distortion.

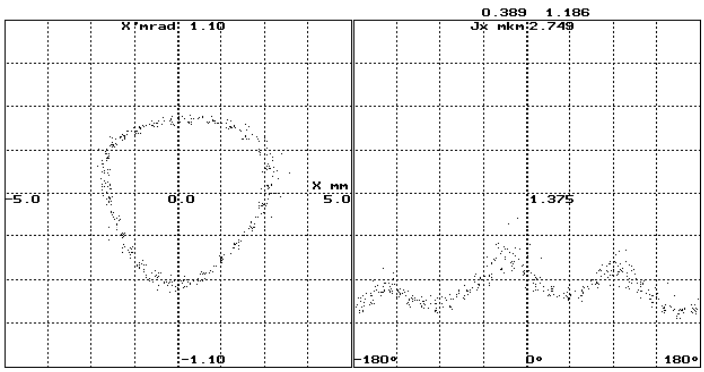

Figure 1: Horizontal phase trajectory measured by two BPMs.

Under the first approach, the displacement $x(n)$ and slope $x'(n) \propto x_{\pi/2}(n)$ of the kicked beam are measured by two BPMs at every turn n and pictured as a phase space plot (Fig.1). A different α_x at BPMs provides the additional distortion of the phase space. Under the second approach when a single BPM station is used, we obtained the beam displacement and slope from the same coordinate array by selecting the pairs of values with $n\pi/2$ phase advance between them. In this case α_x, β_x are the same for both values in each pair and the expression (2) is valid. Applying FFT to the experimental data and using few main harmonics to construct the beam slope and displacement, permits us to reduce drastically the measuring noise and increase the resolution of the phase trajectories distortion. Fig.2 shows the phase space curves near the resonance $3\nu_x = 26$ after FFT for different kick amplitudes. Changing the sextupole strength or the distance from the resonance, we can easily control the distortion (smear) of the phase trajectories. In the vicinity of the resonance $3\nu_x = m$, we can obtain the phase trajectory $J_x(\phi_x)$ as a solution of the following equation [3]

$$\bar{J}_x \simeq J_x - a_{3m} J_x^{3/2} cos3\phi_x,$$

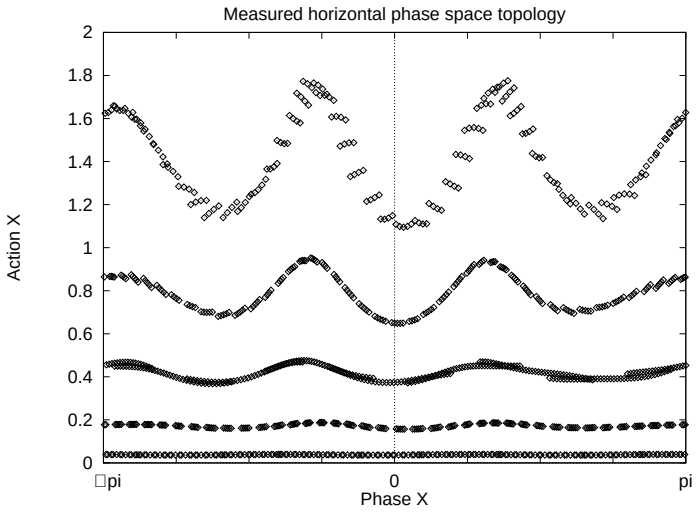

Figure 2: Phase space curves near the resonance $3\nu_x = 26$.

$$a_{3m} \simeq 6\sqrt{2}\frac{A_{3m}}{3\nu_x - m},$$

where $\bar{J}_x = const$ can be found from the initial value of the oscillation amplitude, and A_{3m} is the azimuthal harmonic of the sextupole perturbation

$$A_{3m} = \frac{1}{48}\int_0^{2\pi} \beta_x^{3/2}\mathcal{S}cos(3(\psi_x - \nu_x\theta) + m\theta)d\theta.$$

Here $\mathcal{S}(s) = (d^2B_z(s)/dx^2)/B\rho$ is the normalized sextupole strength. Fig.3 demonstrates

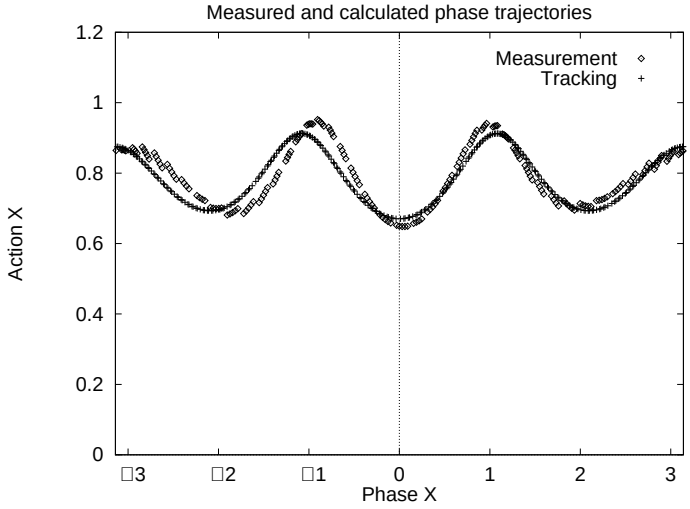

Figure 3: Experimental and simulated phase trajectories.

the agreement between the measured horizontal phase trajectory and the predicted one. The correspondence seems to be quite impressive.

Since the nonlinear perturbation contributes to the phase space distortion at a level of 0.1 mm and less, for further noise reduction we use the data accumulation for the same kick amplitude. For the main harmonic, 10 fold accumulation allows to reduce the rms noise value from 10-20 μm to 4-6 μm. Such a high spectral resolution permits us

to calculate some parameters of the nonlinear system. For instance, we can estimate nonlinear perturbation as

$$a_{3m} = \simeq (J_{max} - J_{min})/(J_{max}^{3/2} - J_{min}^{3/2}) \quad .$$

We extracted the amplitude of the $3\nu_x = 26$ resonance driving term from the measured data and compared it with the calculated from the model Hamiltonian. The agreement seems to be not bad: the experimental value is $A_{3\,26} = -3.1 \pm 1.0$ m$^{-1/2}$, while the theoretical one is $A_{3\,26} = -2.0$ m$^{-1/2}$.

One more nonlinear resonance in our tune region is the resonance $4\nu_x = 35$ that is excited by either octupole perturbation or sextupole perturbation in the second order approximation. Fig.4 shows the phase space topology near and directly at the resonance (two BPMs without harmonic decomposition). An attempt to control the smear of the phase curves near the resonance $4\nu_x = 35$ by sextupoles failed. So, the most probable explanation is that this resonance is driven by the relevant harmonic of the octupole perturbation.

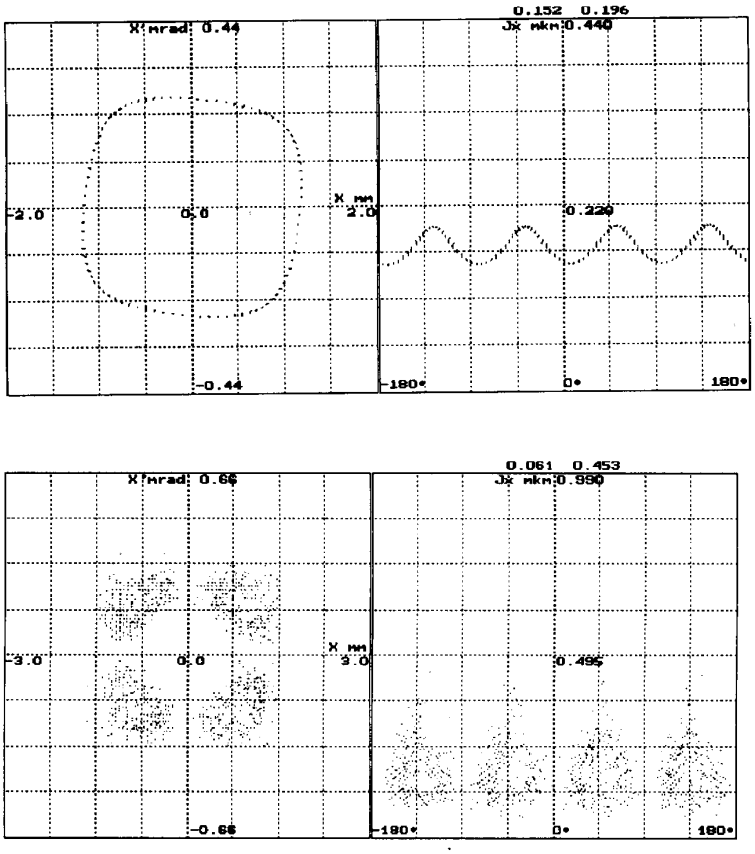

Figure 4: Phase trajectories near and at resonance $4\nu_x = 35$. The plot at the resonance does not use harmonic decomposition.

4 Amplitude dependent tune shift

Nonlinear detuning was studied with the same turn-by-turn technique. The coherent beam oscillations were fired by several kicker pulses with different amplitudes, and tune was extracted from FFT spectrum. The accuracy of the tune measurement is better than $\delta\nu = 2 \cdot 10^{-4}$.

For the Hamiltonian composed of nonperturbed part H_0 and small perturbation H_1

$$H(J, \phi, \theta) = H_0(J) + H_1(J, \phi\theta) \quad , \tag{3}$$

where the perturbation itself consists of constant and oscillated parts

$$H_1(J, \phi\theta) = \bar{H}_1(J) + \tilde{H}_1(J, \phi, \theta) \quad ,$$

the amplitude-dependent tune shift is defined as

$$\Delta\nu(J) = d\bar{H}_1(J)/dJ.$$

For both octupole and sextupole types of perturbation, the nonlinear tune shift is proportionate to the square of the initial beam displacement (Fig.5). A general 2D form of the amplitude dependent tune shift can be expressed as (the second order approximation):

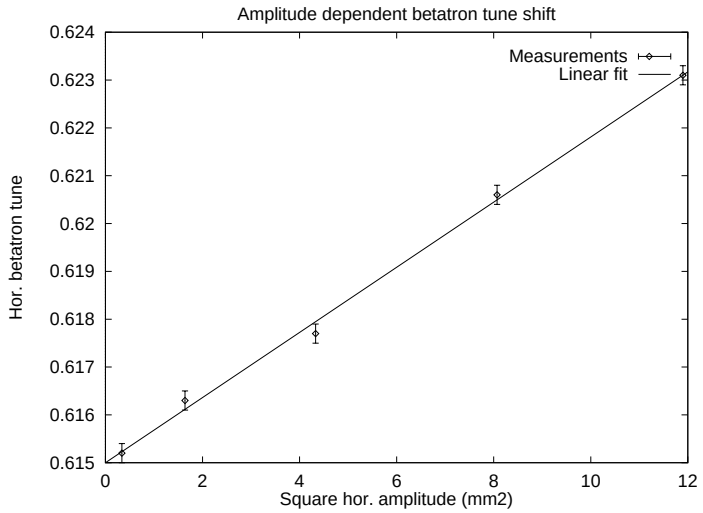

Figure 5: Typical amplitude dependence of the betatron tune.

$$\Delta\nu_x(a_x, a_z) = C_{11}a_x^2 + C_{12}a_z^2,$$
$$\Delta\nu_z(a_x, a_z) = C_{21}a_x^2 + C_{22}a_z^2,$$

where C_{nm} depends on particular perturbative potential. The measured and estimated coefficients values are listed in the Table

$C_{nm} \cdot 10^4$	Theory ($\mathrm{cm}^{-1/2}$)	Experiment ($\mathrm{cm}^{-1/2}$)
C_{11}	0.1	9.0
C_{12}	-0.6	-1.0
C_{21}	-1.9	-4.0
C_{22}	-0.6	-1.0

The difference in theoretical and experimental C_{11} made us explore systematically the horizontal nonlinearity of the ring. We used the difference between octupole and sextupole induced tune shift to distinguish which one defines C_{11} in our case. For the octupole potential, horizontal tune shift is independent of initial tune value and is written as [4]

$$\Delta\nu_x^{(o)}(J_x) = \frac{J_x}{16\pi}\int_0^C \mathcal{O}(s)\beta_x^2(s)ds + o(J_x^2), \tag{4}$$

where C is the machine circumference and $\mathcal{O}(s) = (d^3B_z(s)/dx^3)/B\rho$ is the effective octupole strength. On the contrary, sextupole induced tune shift depends on the initial tune in a resonant way and near the resonance $3\nu_{x0} \simeq m$ can be written as

$$\Delta\nu_x^{(s)}(J_x) \simeq -J_x \cdot 36\ \frac{A_{3m}^2}{3\nu_x - m} + o(J_x^2),$$

$$A_{3m} = \frac{1}{48\pi}\int_0^{2\pi} \beta_x^{3/2}\mathcal{S}\cos(3(\psi_x - \nu_x\theta) + m\theta)d\theta,$$

where $\mathcal{S}(s) = (d^2B_z(s)/dx^2)/B\rho$ is the effective sextupole strength and A_{3m} is the azimuthal harmonic of the sextupole perturbation Hamiltonian.

The horizontal tune shift as a function of the initial tune value ν_{x0} around the resonance $3\nu_{x0} = 26$ (Fig.6, upper) shows that the resulting nonlinear detuning is induced both by sextupole and octupole perturbations. The first demonstrates typical resonant behaviour, while the second produces constant "background" with the value of $\Delta\nu_x^{(o)}/a_x^2 \simeq 8 \cdot 10^{-4}$ mm^{-2}. The octupole correctors SRO and NRO can control the "background" value, while the resonant behavior of the sextupole detuning component remains the same. And vice versa, when we decrease the strength of the strong sextupole lenses in the interaction region and compensate the chromaticity by the sextupole correctors in the arcs, we see that it does not effect the octupole "background" but significantly reduces the sextupole component (together with the resonance width), as shown in Fig.6 (lower).

The source of rather high octupole nonlinearity was not understood yet and a more vigorous study is required. As a probable candidate we consider nonlinear errors in the final focus quadrupoles. As it was shown in [5], the quadrupole edge fields can produce rather large detuning, however, in our case the relevant contribution in C_{11} coefficient is ten times less than the measured one. Fig.7 shows C_{11} versus β_x value in the final focus quadrupoles. This figure demonstrates the parabolic dependence according to (4).

Now, we consider the magnetic field expansion in the median plane of the quadrupole lens [6]:

$$B_z = B_1 x + \frac{1}{5!}B_5 x^5,$$

$$B_n = \frac{d^n B_z}{dx^n}.$$

Introducing the closed orbit distortion at the quadrupole azimuth x_{co}, one can write down for the octupole field component

$$\mathcal{O} \propto B_5 x_{co}^2. \tag{5}$$

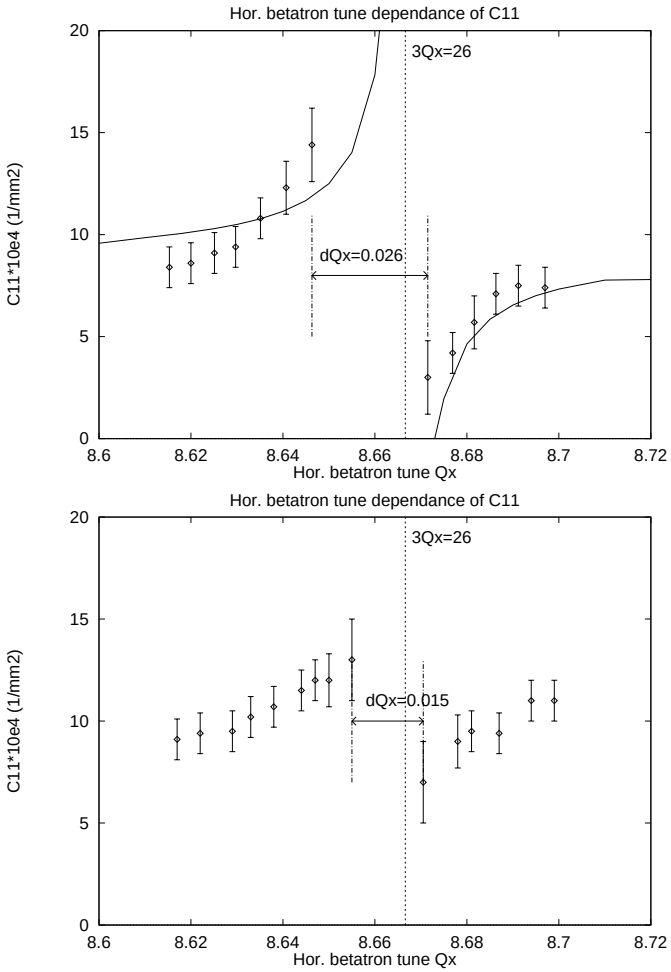

Figure 6: Upper: nonlinear detuning near the resonance $3\nu_x = 26$, solid line – theoretical prediction. Resonance width $\Delta\nu_x = 0.026$; lower: same as upper but with the resonance driving term reduced. Note that the resonance width is decreased in a factor of 2.

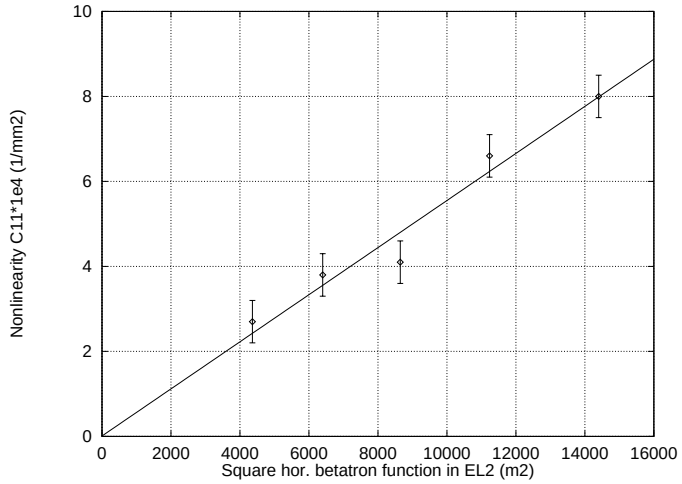

Figure 7: Dependence of the C_{11} coefficient on the β_x value in the final focus quadrupoles.

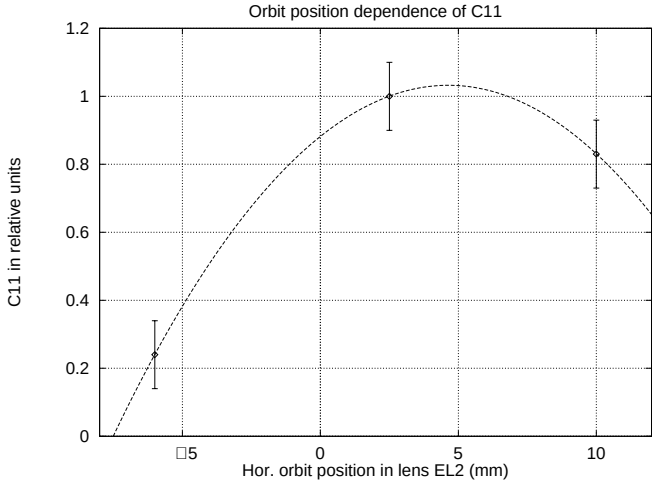

.

Figure 8: Dependence of C_{11} coefficient on the horizontal orbit deviation in the final focus quadrupoles (arbitrary units).

To check this expression we generated a local COD bump at the azimuth of the final focus quadrupoles and measured the horizontal detuning. Fig.8 shows C_{11} versus the horizontal orbit deviation. One can see that the nonlinear detuning depends quadratically on the x_{co}, as it is predicted by (5).

Acknowledgments. We wish to thank I.Ya.Protopopov, the head of VEPP-4M, for providing us with the opportunity to perform the nonlinear experiments, G.Kulipanov and V.Korchuganov for their valuable discussions, A.Kalinin for the turn-by-turn measurement assistance.

References

[1] A. Ando."Distortion of beam emittance with nonlinear magnetic fields", PA 15 (1984), p.177.

[2] A.Kalinin at al. Applications of beam diagnostic system at the VEPP-4 complex. These proceedings.

[3] E. Levichev and V. Sajaev."Nonlinear Dynamics Study of the SIBERIA-2 Electron Storage Ring", AIP Proc.344, p.160-169, 1995.

[4] R.A. Bech, R. Belbeoch and G. Gendreau. Shifts in Betatron Frequencies Due to Energy Spread, Betatron Amplitudes and Closed Orbit Excursions.- Proc. of the Conf. HEAC, Cambridge (1967), A-63.

[5] E.Forest et al. Sources of amplitude-dependent tune shift in the PEP-II design and their compensation with octupoles.- Proc.of EPAC'94, London, 1994, v.2, pp.1033-1035.

[6] K.G.Steffen. High energy beam optics.- Interscience publishers, 1965.

V. Kiselev, E. Levichev,
V. Sajaev, V. Smaluk

Nonlinear beam dynamics study at VEPP-4M

В.А. Киселев, Е.Б. Левичев,
В.В. Сажаев, В.В. Смалюк

Экспериментальное изучение нелинейной динамики на накопителе ВЭПП-4М

ИЯФ 96-67

Ответственный за выпуск А.М. Кудрявцев
Работа поступила 2.10.1996 г.

Сдано в набор 11.10.1996 г.
Подписано в печать 11.10.1996 г.
Формат бумаги 60×90 1/16 Объем 1.8 печ.л., 0.7 уч.-изд.л.
Тираж 200 экз. Бесплатно. Заказ N° 67

Обработано на IBM PC и отпечатано на
ротапринте ГНЦ РФ "ИЯФ им. Г.И. Будкера СО РАН",
Новосибирск, 630090, пр. академика Лаврентьева, 11.